Published in final edited form as:
Cell Calcium. 2013 October ; 54(4): . doi:10.1016/j.ceca.2013.07.002.

Characterization of store-operated Ca^{2+} channels in pancreatic duct epithelia

Mean-Hwan Kim[a,c,1], **Jong Bae Seo**[b], **Lindsey A. Burnett**[b], **Bertil Hille**[b], and **Duk-Su Koh**[a,b,*]

[a]Department of Physics, Pohang University of Science and Technology, Pohang, Republic of Korea

[b]Department of Physiology & Biophysics, University of Washington, Seattle, Washington, USA

Abstract

Store-operated Ca^{2+} channels (SOCs) are activated by depletion of intracellular Ca^{2+} stores following agonist-mediated Ca^{2+} release. Previously we demonstrated that Ca^{2+} influx through SOCs elicits exocytosis efficiently in pancreatic duct epithelial cells (PDEC). Here we describe the biophysical, pharmacological, and molecular properties of the duct epithelial SOCs using Ca^{2+} imaging, whole-cell patch-clamp, and molecular biology. In PDEC, agonists of purinergic, muscarinic, and adrenergic receptors coupled to phospholipase C activated SOC-mediated Ca^{2+} influx as Ca^{2+} was released from intracellular stores. Direct measurement of [Ca^{2+}] in the ER showed that SOCs greatly slowed depletion of the ER. Using IP_3 or thapsigargin in the patch pipette elicited inwardly rectifying SOC currents. The currents increased ~ 8-fold after removal of extracellular divalent cations, suggesting competitive permeation between mono- and divalent cations. The current was completely blocked by high doses of La^{3+} and 2-aminoethoxydiphenyl borate (2-APB) but only partially depressed by SKF-96365. In polarized PDEC, SOCs were localized specifically to the basolateral membrane. RT-PCR screening revealed the expression of both STIM and Orai proteins for the formation of SOCs in PDEC. By expression of fluorescent STIM1 and Orai1 proteins in PDEC, we confirmed that colocalization of the two proteins increases after store depletion. In conclusion, basolateral Ca^{2+} entry through SOCs fills internal Ca^{2+} stores depleted by external stimuli and will facilitate cellular processes dependent on cytoplasmic Ca^{2+} such as salt and mucin secretion from the exocrine pancreatic ducts.

Keywords

Store-operated Ca^{2+} channels; STIM; Orai; TRP; Epithelia; D1-ER cameleon; Ca^{2+} imaging; Patch clamp; RT-PCR

*Corresponding author: Tel: 1-206-543-6661; Fax: 1-206-685-0619; koh@uw.edu, Duk-Su Koh, Department of Physiology and Biophysics, University of Washington, Health Sciences Bldg. Rm. G-424, Seattle, Washington, 98195-7290, USA.
[c]Present address: *The Vollum Institute, Oregon Health & Science University, Portland, Oregon, USA*
[1]These authors contributed equally to this work.

Conflict of interest statement
The authors declare that there are no conflicts of interest.

1. Introduction

Ca^{2+} ions have versatile functions in cellular physiology, such as muscle contraction, neurotransmitter release, hormone secretion, gene expression, and cell proliferation [1]. Intracellular free Ca^{2+} concentration ($[Ca^{2+}]_i$) is kept very low at rest but can be dynamically raised by the opening of Ca^{2+}-permeable ion channels such as IP_3 or ryanodine receptors on the intracellular Ca^{2+} stores and voltage-gated or store-operated Ca^{2+} channels (SOCs) on the plasma membrane [2]. SOCs are one of the major sources for Ca^{2+} influx in many non-excitable and some excitable cells. SOCs are activated by sensing reduced Ca^{2+} levels in the intracellular Ca^{2+} stores following activation of certain G-protein coupled receptors (GPCR).

SOCs seem to be heterogeneous. Their detailed activation profiles and single-channel properties depend upon the cell type [3–6]. This variability suggests diverse molecular compositions, activation mechanisms, and physiological functions. Early studies suggested transient receptor potential (TRP) channels might be the molecular correlate of SOCs [7–8]. Later, two key molecules, the STIM and Orai proteins, were found to better fit the criteria of activation and permeation mechanisms for SOCs [9–10]. They were identified with the Ca^{2+}-release-activated Ca^{2+} current (I_{CRAC}) in mast cells and T lymphocytes, a well characterized class of SOC current. It is proposed that some SOCs distinct from I_{CRAC} may still require TRP channel subunits [11].

Compared to immune cells, the roles and identity of SOCs in epithelial cells are less understood. In epithelia, CaT1 (TRPV6) from the intestine [12] and ECaC (TRPV5) from the kidney [13] were identified as apical Ca^{2+} entry channels. CaT1 has some of the properties of the CRAC channels of the human Jurkat T-lymphocytes [14] and LNCaP prostate cancer cells [15]. Functionally, CaT1 expression is upregulated in diverse pathological conditions, including apoptosis and abnormal cell proliferation [1].

Pancreatic duct epithelial cells (PDEC) have diverse GPCRs coupled to phospholipase C, PIP_2 hydrolysis, and IP_3 generation [16–18]. For example, when protease-activated receptor-2 (PAR-2) is activated by trypsin, initial Ca^{2+} release from stores and delayed Ca^{2+} influx through SOC are observed, and both mechanisms evoke exocytosis and mucin secretion [18]. SOC-mediated Ca^{2+} elevations also decrease the mobility of intracellular organelles including secretory granules and mitochondria [19–20]. Since SOCs are the major and the only known Ca^{2+} entry channels in the non-excitable exocrine epithelia, we here investigated SOC in dog PDEC in detail. Our results indicate that SOC in PDEC is probably composed of STIM/Orai channels that are functionally expressed on the basolateral membrane and tightly regulated by the level of ER Ca^{2+} depletion ($[Ca^{2+}]_{ER}$).

2. Material and methods

2.1. Cell cultures

The epithelial cells originated from the accessory pancreatic duct of a normal dog [21]. Cells grow on Vitrogen-coated Transwell insert (0.7 ml of equal volume mixture of Vitrogen and culture medium), and the inserts were suspended above a confluent feeder layer of cultured human gall bladder myofibroblasts. Cells were maintained at 37°C in 5% CO_2/95% air and fed twice weekly with Eagle's Minimum Essential Medium (EMEM) containing 10% fetal bovine serum, 2 mM L-glutamine, 20 mM HEPES, 2% penicillin/streptomycin solution, 1% insulin-transferrin-sodium selenite medium supplement from Sigma (St. Louis, MO). When confluent, the cells form a tight monolayer (> 1 kOhm/cm^2) and show polarized expression of GPCRs and ion channels [21–23]. For subculture, the cells in a monolayer were treated with 0.05% trypsin/EDTA at 37°C for 45 min and passaged to newly coated inserts with

fresh feeder layers. Cells of passage number 10–30 were used for studies. For single-cell experiments, cells were plated on 5 mm round coverglasses coated with a thick layer of Vitrogen and used for measurement after 2–4 days. These subconfluent epithelial cells were presumably not completely differentiated or polarized.

2.2. Solutions and chemicals

Normal Ringer's solution, used in most experiments, contained (in mM): 137.5 NaCl, 2.5 KCl, 2 $CaCl_2$, 1 $MgCl_2$, 10 D-glucose and 10 HEPES, pH 7.3. In Ca^{2+}-free Ringer's solution, $CaCl_2$ was omitted and 100 μM EGTA was added to remove contaminating free Ca^{2+}. Dimethyl sulfoxide was used to prepare stock solution of 5 mM thapsigargin. Fura-2 AM was from Molecular Probes (Eugene, OR). Other chemicals and culture reagents were from Sigma (St. Louis, MO). Solution exchange was achieved with a local perfusion system that allowed complete exchange within 0.5 s. All experiments were performed at room temperature (22–24°C).

2.3. Fluorescence measurements of Ca^{2+}

To measure $[Ca^{2+}]_i$ in single cells, PDEC were loaded with 2 μM of the membrane-permeant Ca^{2+}-sensitive dye Fura-2 AM for 30 min. Single cells were excited at 340 nm and 380 nm at 1 or 2 s intervals and the emitted fluorescence at 510 nm detected using CCD camera (Pixelfly; PCO-TECH Inc, Romulus, MI). A cell-free region was used for background fluorescence correction. $[Ca^{2+}]_i$ was calculated as $K^* \times (R-R_{\min})/(R_{\max}-R)$, where R is the ratio of fluorescence at 340 nm/ fluorescence at 380 nm, K^* is the effective dissociation constant, and R_{min} and R_{max} are the ratios at minimal and maximal $[Ca^{2+}]_i$. R_{min}, R_{max}, and K*, determined with cells perfused with K^+-rich external solutions containing 20 μM ionomycin and 5 μM thapsigargin plus 20 mM EGTA or 15 mM Ca^{2+}, or 20 mM EGTA and 15 mM Ca^{2+}, were 0.334, 3.733, and 2874 nM, respectively (n = 10–14 cells for each measurement). For $[Ca^{2+}]_i$ with polarized PDEC, monolayers grown in Snapwell inserts (Cat. No. 3407; Corning Costar, Tewksbury, MA) were loaded with 4 μM Fura-2 AM for 30 min and then mounted on top of a customized chamber made with a glass slide. In this chamber the apical and basolateral sides are separately perfused. The result is presented as fluorescence ratio (F340/F380 nm) since no cell-free region was present for background subtraction.

In order to monitor the Ca^{2+} level within the ER Ca^{2+} stores ($[Ca^{2+}]_{ER}$), we used a genetically encoded, ER-targeted Ca^{2+} indicator, D1-ER cameleon (kind gift from Dr. R.Y. Tsien, University of California) [24]. cDNA of D1-ER cameleon (1 μg/ 30 mm dish) was transfected into PDEC for 6 hrs with X-tremeGENE 9 DNA Transfection Reagent (Roche Applied Science, Indianapolis, IN). Cells expressing the fluorescent probes were measured with a Zeiss 710 laser-scanning confocal microscope 1–2 days after transfection. For this fluorescence resonance energy transfer (FRET)-based probe, cyan fluorescence protein (CFP) was excited at 405 nm and emission was detected at 420–481 nm. Yellow fluorescence protein (YFP) was excited by the CFP emission and its fluorescence was detected at 560–616 nm. The uncalibrated result is given as the FRET ratio, YFP emission divided by CFP emission.

2.4. Fluorescence microscopy of Orai1-Orange and STIM1-GFP

Cells were transfected with cDNAs as pairs of Orai3-GFP/STIM1-YFP or Orai1-orange/ STIM1-GFP (1 μg each/ 30 mm dish for single cells and 3 μg each/ 100 mm dish for PDEC monolayers. All constructs based on human sequences were kind gifts from Dr. M. Cahalan, University of California, Irvine and Dr. L. Chen, Peking University) and monitored with a Zeiss 710 confocal microscope (63× 1.49-NA objective). Orai3-GFP was excited at 488 nm and the emission was detected at 492–516 nm, while STIM1-YFP was excited at 514 nm

and the emission was recorded at 518–621 nm. For the Orai1/STIM1 pair, we used respectively orange (ex. 514 nm, em. 550 – 681 nm) and GFP (ex. 488, em. 492 – 543 nm) channels. These protocols minimize the cross-over of fluorescence signals between channels. Colocalization of the two probes was estimated using Pearson's analysis implemented in Nikon Elements software (Nikon Instruments Inc., Melville, NY, USA). Pearson's linear correlation coefficient (r_P) measures the mean overlap of pixels with two different colors:

$$r_P = (\sum((A_i - A_{\text{avg}})(B_i - B_{\text{avg}}))) / \sqrt{(\sum(A_i - A_{\text{avg}})^2 \sum(B_i - B_{\text{avg}})^2)},$$

where A_{avg} and B_{avg} are the averages of A and B colors, respectively, and i is the i-th pixel of the image. r_P ranges from −1 to +1. Values of +1 and −1 suggest perfect positive and negative correlation between two variables, respectively. Considering the values obtained in single-cell and monolayer experiments, we set the cut-off criterion for significant colocalization of two colors at 0.25. It is known that STIM1 in the ER translocates toward Orai1 in the plasma membrane after store depletion, and the membrane of PDEC is enriched at the cell periphery in confocal images. Therefore regions of interest (ROIs) for Pearson's analysis were allocated mainly at the cell boundary.

2.5. Patch-clamp recording

Whole-cell patch-clamp recording was performed with an EPC-9 amplifier (HEKA Elektronik). Pipette resistance was 3–7 MΩ. The current signals were low-pass filtered at 1 kHz and sampled at 5 kHz. The divalent-free external solution used in patch-clamp experiments contained (mM): 140 NaCl, 5 EDTA, 10 glucose, and 10 HEPES with pH 7.3. The pipette solution contained (mM): 135 Cs-glutamate, 3 $MgCl_2$, 10 EGTA, and 10 HEPES with pH 7.3. The experiments shown in Figure 3E and F used 6 mM instead of 3 mM $MgCl_2$. The composition of 20 mM Ca^{2+}-containing Ringer's solution is (mM): 20 $CaCl_2$, 135 N-methyl-D-glucamine, 135 methanesulfonic acid, 10 HEPES, and 10 glucose (methanesulfonic acid was the main anion in the external solution to reduce currents through Cl^- channels [25]). Currents were measured using a voltage-ramp protocol; membrane potential was held at 0 mV and jumped down to −100 mV for 50 ms and then ramped up to +100 mV over 200 ms. Development of SOC-mediated current was monitored by applying the voltage ramps every 2 s.

2.6. Reverse transcription-PCR (RT-PCR)

Total RNA was isolated from polarized PDEC with PureLink® mini kit (Invitrogen, Grand Island, NY) according to the manufacturer's instructions. First-strand cDNA was synthesized by reverse transcription of 2 μg of total RNA with SuperScript® III First-Strand Synthesis System (Invitrogen) following standard protocols. We purchased a dog pancreatic cDNA library from Zyagen Laboratories (San Diego, CA). cDNAs were then subjected to polymerase chain reaction (PCR). Primer sequences for Orai, STIM, and TRP channel subtypes and the expected size of PCR products are described in Table 1. PCRs were run on PerkinElmer 2400 Geneamp PCR machine (Waltham, MA) in a final volume of 20 μL containing 1 μL of the first strand cDNA, 1 unit DNA polymerase (Platinum® Pfx DNA polymerase, Invitrogen) and each primer (200 nM). Conditions of DNA amplification included an initial denaturation step of 5 min at 94°C, and 35 cycles of 30 s at 94°C, 30 s at 55°C, 30 s at 68°C, and finally 7 min at 68°C. Finally reaction products were separated on a 2% agarose gel, stained with ethidium bromide, and photographed.

2.7. Data analysis

Numerical values are given as mean ± standard error of mean (SEM); *n* is the number of cells measured, unless otherwise stated. Error bars shown in averaged SOC currents are SEM and they are omitted for average traces of intracellular and ER Ca^{2+} due to relatively high sample rates. Statistically significant differences ($P \leq 0.05$ [*]) between means of two groups were determined by Student's two-tailed, unpaired *t*-test.

3. Results

3.1. Activation of SOCs by endogenous GPCRs in PDEC

The pancreatic epithelium is innervated by sympathetic and parasympathetic inputs releasing catecholamines and acetylcholine, respectively [26–27], and PDEC receive other external stimuli, including ATP that is released from pancreatic acinar cells [28]. Accordingly, among other G-protein coupled receptors (GPCRs), PDEC express purinergic, adrenergic, and cholinergic receptors [17,21,23], some of which are coupled to G_q. They activate PLC, leading to IP_3 generation, depletion of internal Ca^{2+} stores, and activation of SOCs. Therefore we looked at the GPCR-induced Ca^{2+} entry through SOCs with Ca^{2+}-photometry (Fig. 1). To dissect Ca^{2+} influx through SOCs from Ca^{2+} release by intracellular stores, we compared $[Ca^{2+}]_i$ rises in the presence and absence of extracellular Ca^{2+}. When cells were treated with 100 μM UTP to activate endogenous purinergic receptors in a Ringer's solution containing 2 mM Ca^{2+}, $[Ca^{2+}]_i$ rose from a low resting level (~100 nM) to a peak of several micromolar within a few seconds (solid line in Fig. 1A, [17]). After reaching the peak, $[Ca^{2+}]_i$ started to fall rapidly, followed by a second hump that decreased slowly over several minutes to a steady level. When cells were preincubated with a high concentration of 2-APB (100 μM), a SOC blocker, the secondary slow signal was removed, suggesting delayed Ca^{2+} influx through SOC (Supplementary Fig. 1A). Similarly, in our previous study, La^{3+} inhibited the SOC-mediated secondary Ca^{2+} rise [18]. When extracellular Ca^{2+} was omitted (dotted line), the Ca^{2+} signals showed a similar initial peak response but decayed more quickly without slow components. In PDEC, UTP activates only G_q-coupled $P2Y_2$ receptors, whereas ATP activates both $P2Y_2$ (coupled to G_q only) and $P2Y_{11}$ (coupled to G_q and G_s) receptors. Thus $P2Y_{11}$ receptors increase both intracellular Ca^{2+} and cAMP levels [17]. Since ATP elicited a Ca^{2+} response similar to that with UTP, we conclude that any cAMP does not change Ca^{2+} signals significantly (Fig. 1B).

To test whether adrenergic stimulation also increased cytoplasmic $[Ca^{2+}]$, we treated PDEC with 1 μM epinephrine (Fig. 1C). In the presence of external Ca^{2+}, $[Ca^{2+}]_i$ increased slowly to a small peak followed by a slow decline towards a steady-state (solid line). Without Ca^{2+} in the external medium, epinephrine evoked no rise of $[Ca^{2+}]_i$ (dotted line). Similarly the cholinergic agonist acetylcholine (100 μM) elicited only a slow $[Ca^{2+}]_i$ increase (Fig. 1D). A lower concentration (10 μM) evoked a comparative weak $[Ca^{2+}]_i$ response (data not shown).

We took the difference between the $[Ca^{2+}]_i$ rise in the presence and absence of external Ca^{2+} (Fig. 1E) to estimate Ca^{2+} influxes through SOCs for the different agonists. For ATP and UTP, the difference develops rather quickly as Ca^{2+} is being released from stores. For epinephrine and acetylcholine, the delayed Ca^{2+} influx is small and slow.

3.2. Activation of SOCs by depletion of intracellular stores in PDEC

Next we examined loss of Ca^{2+} from the stores directly. We expressed D1-ER cameleon, a genetically encoded probe that reports endoplasmic reticulum (ER) Ca^{2+} concentration ($[Ca^{2+}]_{ER}$) [24]. There was an abrupt decrease of $[Ca^{2+}]_{ER}$ upon UTP stimulation (Fig. 2A). The loss was much smaller in 2 mM Ca^{2+} Ringer's solution (black line) than in Ca^{2+}-free Ringer's (gray line), suggesting that the ER is actively being refilled as Ca^{2+} enters through

SOCs. After the agonist was removed, $[Ca^{2+}]_{ER}$ recovered only if there was SOC-mediated Ca^{2+} entry. Block of SOC with 100 μM 2-APB removed ER Ca^{2+} refilling (Supplementary Fig. 1B).

In contrast to purinergic activation, epinephrine depleted $[Ca^{2+}]_{ER}$ very little, confirming that ER depletion is a prerequisite for SOC activity (Fig. 2B). Nevertheless this minor depletion of ER activates a small component of SOC and mediates minor but detectable Ca^{2+} influx when extracellular Ca^{2+} is available (Figs. 1C and E). After treatment with epinephrine in 2 mM Ca^{2+}, a significant decrease of $[Ca^{2+}]_{ER}$ could still be initiated by 50 μM BHQ, a sarcoplasmic-endoplasmic reticulum Ca^{2+}-ATPase (SERCA) inhibitor (Fig. 2D, red line). The $[Ca^{2+}]_{ER}$ is clearly in dynamic balance between pump and release mechanisms.

To estimate the contribution of Ca^{2+} entry to store refilling, we subtracted the $[Ca^{2+}]_{ER}$ trace in the absence of external Ca^{2+} from that in the presence (Fig. 2C-a). This difference developed quickly and reached a peak about 2 min after activation of the purinergic receptors. A much smaller and gradual increase of the difference trace for epinephrine suggests only weak refilling by SOCs during adrenergic stimulation (Fig. 2C-b). Finally, Figure 2E compares the SOC-related $[Ca^{2+}]$ increase in cytoplasm ('Cyto' from Fig. 1E-a, red line) with that in the ER ('ER' from Fig. 2C-a, blue line) during purinergic stimulation. The two curves track each other, rising quite rapidly and peaking within 1–2 min.

Whole-cell patch-clamp allowed us to record SOC channel current directly (Fig. 3A). In order to deplete the Ca^{2+} stores, the patch-pipette solution included 100 μM IP_3 to release Ca^{2+} and 10 mM EGTA to chelate the released Ca^{2+}. In addition, the external solution contained 20 mM Ca^{2+} to increase SOC conductance. After breakthrough into whole-cell configuration (at time zero), currents developed with a time constant of ~28 s (Fig. 3A, currents measured at −100 mV). They reached a maximal level at ~50 s and then slowly inactivated over a couple of minutes, presumably through Ca^{2+}-dependent channel inactivation [29]. When SOC current was measured in a ramp voltage protocol varying from −100 mV to 100 mV (Fig. 3B), the current-voltage relationship exhibited the typical inward rectification of SOC current [30]. Similarly, thapsigargin, an irreversible inhibitor of the SERCA pump that induces store depletion, also slowly activated inwardly rectifying SOC (Figs. 3C and D). In PDEC, the SOC current density during IP_3 receptor activation (0.8 ± 0.2 pA/pF at −100 mV, $n = 5$) is comparable to that for other epithelia (~ 2.5 pA/pF at −100 mV, [15]) and for Jurkat T cells (~ 1 pA/pF at −80 mV, [31]; see also [15]). In PDEC, thapsigargin-mediated SOC currents increased ~8-fold in a divalent-free external solution ($n = 3$, Figs. 3E and F) as is found for many SOCs and CRAC currents in other cells [31]. Thus the SOC-mediated currents in our epithelial cells are similar to those in other cell types in terms of dependence on depletion of Ca^{2+} stores, current-voltage relations, and ion permeability.

3.3. Pharmacological block of SOCs in PDEC

The pharmacology of store-operated Ca^{2+} entry is quite variable [3–6]. We compared three standard inhibitors using cytoplasmic Ca^{2+} photometry (Fig. 4). In these experiments, SOCs were fully activated by pre-incubating cells with 5 μM thapsigargin for 5 min before recording. Initially, cells were bathed in a Ca^{2+}-free Ringer's solution, and then Ca^{2+} influx through the SOCs was elicited by applying 2 mM Ca^{2+} Ringer's solution (Fig. 4A, see also [18]). The thapsigargin-induced Ca^{2+} influx was reversibly blocked both by 10 and by 100 μM 2-aminoethoxydiphenyl borate (2-APB) (Figs. 4A and D). We found the same result for the human pancreatic duct epithelial cell lines PANC1 and CFPAC (data not shown). Similarly, La^{3+} reduced Ca^{2+} influx in a dose-dependent manner (Figs. 4B, C, and D), with half-maximal inhibition at 199 nM La^{3+} (Fig. 4C). Finally, SKF-96365 at 50 μM, found to

be supramaximal concentration for SOCs in other cell types, blocked only ~50% of Ca^{2+} influx (Fig. 4D). In whole-cell patch-clamp recordings (Supplementary Fig. 2), the thapsigargin-induced monovalent currents were effectively blocked by La^{3+}. The La^{3+} sensitivity was similar to that in Figure 4C for block of Ca^{2+} entry. 2-APB at 100 μM completely and reversibly blocked the current as SOC-mediated Ca^{2+} influx. However, 10 μM 2-APB did not inhibit but, rather, slightly increased the current ($P = 0.05$, Supplementary Fig. 2B).

3.4. Basolateral localization of SOCs in PDEC

In differentiated PDEC, several ion channels and transporters are selectively localized on either apical or basolateral sides for vectorial ion transport [32]. Some GPCRs exhibit such a polarized distribution, making them able to respond to the agonists on a specific side of the monolayer. For example, $P2Y_{11}$ receptor, protease-activated receptor 2 (PAR-2), and histamine receptor are localized on the basolateral membrane, whereas $P2Y_2$ receptor is expressed on both sides [16,22,23]. To investigate the localization of SOCs, we monitored the SOC-mediated $[Ca^{2+}]_i$ increase in polarized PDEC monolayers while solutions containing different external Ca^{2+} concentrations were perfused into the apical and basolateral sides independently (Fig. 5). In this experiment, SOCs were fully activated by thapsigargin. After recording the basal $[Ca^{2+}]_i$ level with a Ca^{2+}-free Ringer's solution on both sides, either the apical/luminal or basolateral/serosal sides were supplied with 2 mM Ca^{2+}. $[Ca^{2+}]_i$ increased only with basolateral Ca^{2+} application and not with apical application. Thus, functional SOCs are restricted to the basolateral membrane of PDEC.

3.5. Expression of candidate SOC genes in PDEC

The concept of 'capacitative' or 'store-operated' Ca^{2+} entry was proposed almost 30 years ago [33] (see also [34]). Underlying molecules were later discovered using RNAi-based genetic screening [35–36]. STIM1 and STIM2 are proteins on the ER membrane that sense the Ca^{2+} level in the ER lumen. After depletion of Ca^{2+} in the Ca^{2+} store, the STIM proteins aggregate in regions just beneath the plasma membrane to communicate with Orai proteins that form Ca^{2+}-permeable channels. There are three mammalian subtypes, Orai1, Orai2 and Orai3. To monitor the expression of STIM and Orai, we designed primers for RT-PCR based on mouse and human sequences (Table 1). We find that the genes for STIM1, STIM2, Orai1, Orai2, and Orai3 are all expressed in dog PDEC (Figs. 6A and B). When compared using quantitative PCR, Orai3 is the dominant subtype of Orai channels (Supplementary Fig. 7A). Dog pancreatic tissue also expressed all STIM and Orai subtypes (Supplementary Fig. 3). STIM and Orai also complex with and activate some TRP channels [11,36] that had been proposed as the candidates of SOC channels [37]. Therefore we tested the expression of a few TRP channels. TRPC1 and TRPV6 were clearly detected in dog PDEC (Fig. 6C) and in human pancreatic duct epithelial cell lines (CAPAN-1, PANC-1, and CFPAC; data not shown). The expression level of TRPC3 in dog PDEC was very low, and TRPC4 was not detected by the primers we designed (data not shown).

3.6. Aggregation of STIM and Orai proteins upon store depletion

To visualize subcellular behavior of STIM and Orai proteins, we over-expressed fluorescent STIM1-YFP and Orai3-GFP both in single dissociated PDEC (Fig. 7) and in differentiated PDEC monolayers (Supplementary Figs. 4A and B). Cells were imaged in normal Ringer's solution (0 min) and then treated with 5 μM thapsigargin in Ca^{2+}-free Ringer's solution. For single isolated cells, sequential confocal images demonstrated that both STIM and Orai formed puncta after thapsigargin treatment and that the YFP and GFP puncta became colocalized (Fig. 7A). We calculated the Pearson correlation coefficient (r_P) to estimate colocalization of the two colors pixel-by-pixel (see Materials and Methods, 2.4). In all cells, r_P increased after depletion of the Ca^{2+} stores by application of thapsigargin over 3 – 10 min

(Fig. 7B, $r_P = 0.20 \pm 0.03$ in the resting cells vs. $r_P = 0.66 \pm 0.02$ at 10 min). Similar experiments with polarized PDEC monolayers growing on a filter membrane were technically more challenging due to high background fluorescence from the plastic membrane and the height fluctuations of the membrane during perfusion. Therefore, we compared the before and after colocalizations in different sets of Transwells. Nevertheless, puncta of Orai3-GFP and STIM1-YFP were detected in all 16 tested cells, and their colocalization increased after store depletion (Supplementary Fig. 4A and B). 14 out of 16 cells qualified as showing significant colocalization of the probes, if we set the cut-off value as $r_P > 0.25$. Average r_P values were 0.20 ± 0.01 for the resting cells and 0.67 ± 0.01 for thapsigargin-treated cells. Colored Orai1 and STIM1 behaved similarly at both single cells and monolayers (Supplementary Figs. 5 and 6). We further attempted to localize the puncta formation of endogenous Orai channels with immunocytochemical staining of polarized PDEC using an Orai3 antibody (Supplementary Fig. 4C). After store depletion, the Orai3 puncta seemed to be formed at the lateral membrane but not at the apical or basal sides of polarized PDEC. However the exact localization of functional SOCs in dog PDEC warrants further investigation due to a relatively low profile and overlap of the cells in monolayers. In sum, our results suggest that STIM and Orai proteins coassemble in both single PDEC and polarized monolayers after thapsigargin treatment.

Our results including activation after store depletion, sensitivity to pharmacological blockers, and colocalization of exogenous Orai1/3 and STIM1, suggest that SOCs are composed of Orai and STIM proteins. To test this hypothesis, we knocked down the expression of Orai3, the most abundant Orai subtype (Supplementary Figs. 7B-D). Out of 3 siRNA sequences, one sequence (‘S1’) was found to be most efficient to reduce Orai3 gene expression (Supplementary Fig. 7B). Considering the transfection efficiency with PDEC (<50%), reduction of gene expression by 50% may suggest a complete removal of Orai3 messages. In functional assays of SOCs in single PDEC, we cotransfected Ds-Red proteins to select transfected cells. Ds-Red positive cells were regarded as cells transfected with Orai3-S1 sequence. On average, the cells with Ds-Red showed less Ca^{2+} influx upon 2 mM Ca^{2+} treatment (Supplementary Figs. 7C and D). However some ‘transfected’ cells did show almost the same Ca^{2+} rise as untransfected or mock-transfected cells. These results suggest possible contribution or compensation by Orai1 and 2 expressed in PDEC.

4. Discussion

We have characterized SOCs in pancreatic duct epithelial cells and show that they share several features with the classical CRAC channels of immune and epithelial cells. The SOCs of PDEC are activated by diverse physiological stimuli and are localized to the basolateral membrane in differentiated monolayers. PDEC express STIM and Orai, candidate proteins for SOC, and show aggregation and colocalization of STIM and Orai in puncta during store deletion.

4.1. SOCs in other cell types

In non-excitable cells, which lack voltage-sensitive Ca^{2+} channels, it is believed that SOCs have an important function in cytoplasmic Ca^{2+} regulation. For example, CRAC channels are critically involved in mitogenesis and differentiation of immune cells [38], and impaired Ca^{2+} influx through CRAC underlies several inherited immunodeficiency diseases [39]. The physiological role of SOCs in non-excitable cells other than immune cells is relatively less characterized. Inappropriate epithelial Ca^{2+} entry channels in prostate epithelial cells are proposed to promote prostate cancer [15]. Pancreatic β-cells [40] and acinar cells [41] also have functional SOCs, which may contribute to the PCR signals for STIM and Orai that we found in generic pancreatic tissue (Supplementary Fig. 3). Functional expression of SOCs is also reported in excitable cells [42–43].

4.2. SOCs in PDEC

Physiological activation of SOCs in pancreatic ducts should occur as neurotransmitters and ATP are released from nearby nerve terminals and from neighboring cells (Fig. 1) [26–28]. It has been shown that muscarinic input from parasympathetic terminals modifies ductal secretion [27]. Weak $[Ca^{2+}]_i$ response to acetylcholine (Fig. 1D) suggests that our PDEC from the main duct have weak muscarinic signaling and perhaps express a low level of receptors. As compared to the pharmacology of SOCs expressed in some other cells, SOCs in PDEC may show slightly different characteristics. Apparently the effects of 2-APB depend on the molecular composition of SOC channels in expression systems with specific Orai and STIM subtypes. Low concentrations of 2-APB may be stimulatory, and high concentrations, inhibitory [44–46]. Monovalent SOC currents measured with divalent-free solution in PDEC were potentiated by 10 μM 2-APB but abolished by 10 μM 2-APB (Supplementary Fig. 2). However, both low (10 μM) and high (100 μM) concentration of 2-APB significantly blocked Ca^{2+} influx through thapsigargin-induced SOC channels of PDEC (Fig. 4). We have no clear explanation for the discrepancy between Ca^{2+} imaging and current measurements at 10 μM 2-APB at present. Possibly, 2-APB increases the permeability ratio between Cs^+ and Ca^{2+} and (P_{Cs}/P_{Ca}) so that activated SOCs become less Ca^{2+}-permeable as observed with Orai3 currents [47]. Alternatively, 2-APB inhibits SOC but activates another Ca^{2+}-impermeable channels in dog PDEC. Overall 2-APB is not a clean blocker, especially at low concentration. We therefore used 100 μM APB to block SOC-mediated Ca^{2+} influx (Supplementary Fig. 1).

We also found that another commonly used blocker, SKF-96365 (50 μM), blocked the $[Ca^{2+}]_i$ rise only partially (~ 50%; Fig. 4D) in PDEC. All these possible small differences may reflect different combinations of Orai, STIM, and TRP proteins [48] (see below for further discussion).

4.3. Molecular identity of SOCs in PDEC

The initial discovery of STIM and Orai proteins led to the concept that STIM senses the depletion of ER Ca^{2+} and aggregates and interacts with Orai in the plasma membrane to activate the channels [34]. STIM1 is suggested to activate SOCs during receptor stimulation, whereas STIM2 may maintain resting Ca^{2+} levels [49]. Dog PDEC expressed both STIM subtypes. Interestingly, STIM1 can form complexes with both TRPC1 and Orai1 upon store depletion, but knockdown of Orai1 completely abrogates TRPC1 function [11]. Therefore it is hypothesized that the Orai1/STIM1 complex may form the primary channel during store depletion, and then TRPC1 contributes to the summed Ca^{2+} entry. The status of TRP channels and the functional relationship between Orai and TRP channels in store depletion remains controversial [11]. PCR screening showed expression of Orai1 and TRPC1 in dog PDEC, leaving the possibility of their interaction to form functional SOC channels. We also detected TRPV6 (Fig. 6C) that has been previously reported as a 'Ca^{2+} transporter protein (CaT1)' that functions in Ca^{2+} absorption in apical intestine. Similarly, TRPV5, 'Epithelial Calcium channel (ECaC)' also enhances apical Ca^{2+} re-absorption in renal membranes and kidney [13]. Previously, TRPV6 had been proposed to be a part of CRAC channels [14]. The evidence for a molecular link between STIM and TRPV6 proteins seem weaker than for between STIM1/Orai1/TRPC1 [50].

Our PDEC express Orai2 and 3 in addition to Orai1, suggesting their potential contribution to functional SOCs in PDEC. Orai3, the major subtype in dog PDEC (Supplementary Fig. 7A), has a different sequence from that of Orai1, particularly in the regions of pore-forming domains, so that pores with Orai3 show unique features in gating, ion selectivity and activation [51]. Orai3 coupled to STIM1 showed an inactivation index, defined as steady-state current divided by peak current, lower than that of the Orai1/STIM1 complex (0.28 vs

0.61, [48]). This value matches well with our results (0.28 ± 0.05, $n = 14$, Fig. 3E) consistent with the significant expression of Orai3 in dog PDEC. In sum, SOCs in dog PDEC might be formed by combinations of multiple subtypes of STIM and Orai. We also can not exclude that TRP participates, since some TRP genes are expressed. This issue needs further investigation.

4.4. Function of SOCs in PDEC

In differentiated epithelial cells, the expression of membrane proteins is polarized. We find that SOCs in PDEC are expressed on the basolateral membrane as reported for pancreatic acinar cells [41] and polarized human bronchial and colonic epithelial cells [52]. Mogami et al. (1997) [41] showed that these basolateral SOCs help to replenish the Ca^{2+} stores that have a significant role in apical secretion. The SOCs are tightly coupled to the Ca^{2+} store underneath the basolateral membrane. Ca^{2+} coming in through SOCs is efficiently transferred into the Ca^{2+} store by SERCA pumps without significant rise of the global cytoplasmic Ca^{2+} concentration. The authors proposed that the Ca^{2+} is transported through an “ER tunnel” connecting basal and apical sides to trigger Ca^{2+}-dependent exocytosis of apical zymogen granules. Alternatively, a recent study localizing Orai and STIM proteins after ER depletion suggests that functional SOCs may be localized in the lateral membrane near to the tight junction, which allows apical Ca^{2+} to rise without any sophisticated tunneling system [53]. Our immunohistochemical staining of Orai3 puncta supports this possibility. In pancreatic duct, similar mechanisms with SOC channels may efficiently replenish Ca^{2+} in the stores. Indeed, we show that $[Ca^{2+}]_{ER}$ depletes faster and much more extensively when Ca^{2+} influx through SOCs is absent, suggesting that ER refilling is strong and starts surprisingly early during purinergic stimulation. It would be interesting to investigate how this refilling by basolateral SOCs promotes apical mucin exocytosis and HCO_3^- secretion [32]. SOC-mediated Ca^{2+} signaling and secretion in both acinar and duct cells of the pancreas may also contribute to pathological conditions such as pancreatitis by aberrant Ca^{2+} signaling through Ca^{2+} influx [54].

Supplementary Material

Refer to Web version on PubMed Central for supplementary material.

Acknowledgments

We thank Evelyn Tong, Thomas Wong for technical assistance, Claudia Moreno for helpful discussion, and Eamonn Dickson, and Toan G. Nguyen for comments on manuscripts. This work was supported by grants from the National Institutes of Health Grant (DK080840 to D.S.K., GM83913 and NS08174 to B.H.) and from the Korea Research Foundation (KRF-2006-612-C00011 and KRF-2008-357-E00032 to M.H.K.).

Abbreviations in this paper

IP_3	inositol 1,4,5-trisphosphate
ATP	adenosine-5′-triphosphate
UTP	uridine-5′-triphosphate
SOCs	store-operated Ca^{2+} channels
PDEC	pancreatic duct epithelial cells

References

1. Berridge MJ, Lipp P, Bootman MD. The versatility and universality of calcium signalling. Nat Rev Mol Cell Biol. 2000; 1:11–21. [PubMed: 11413485]

2. Bootman, MD.; Berridge, MJ.; Putney, JW.; Roderick, HL., editors. Calcium signaling. Cold Spring Harbor Laboratory Press; 2012. p. 499
3. Vanden Abeele F, Lemonnier L, Thebault S, Lepage G, Parys JB, Shuba Y, Skryma R, Prevarskaya N. Two types of store-operated Ca^{2+} channels with different activation modes and molecular origin in LNCaP human prostate cancer epithelial cells. J Biol Chem. 2004; 279:30326–30337. [PubMed: 15138280]
4. Albert AP, Large WA. Store-operated Ca^{2+}-permeable non-selective cation channels in smooth muscle cells. Cell Calcium. 2003; 33:345–356. [PubMed: 12765681]
5. Liu X, Groschner K, Ambudkar IS. Distinct Ca^{2+}-permeable cation currents are activated by internal Ca^{2+}-store depletion in RBL-2H3 cells and human salivary gland cells, HSG and HSY. J Membr Biol. 2004; 200:93–104. [PubMed: 15520907]
6. Trepakova ES, Gericke M, Hirakawa Y, Weisbrod RM, Cohen RA, Bolotina VM. Properties of a native cation channel activated by Ca^{2+} store depletion in vascular smooth muscle cells. J Biol Chem. 2001; 276:7782–7790. [PubMed: 11113149]
7. Lievremont JP, Bird GS, Putney JW Jr. Canonical transient receptor potential TRPC7 can function as both a receptor- and store-operated channel in HEK-293 cells. Am J Physiol, Cell Physiol. 2004; 287:C1709–C1716. [PubMed: 15342342]
8. Zeng F, Xu SZ, Jackson PK, McHugh D, Kumar B, Fountain SJ, Beech DJ. Human TRPC5 channel activated by a multiplicity of signals in a single cell. J Physiol (Lond). 2004; 559:739–750. [PubMed: 15254149]
9. Roos J, DiGregorio PJ, Yeromin AV, Ohlsen K, Lioudyno M, Zhang S, Safrina O, Kozak JA, Wagner SL, Cahalan MD, Velicelebi G, Stauderman KA. STIM1, an essential and conserved component of store-operated Ca^{2+} channel function. J Cell Biol. 2005; 169:435–445. [PubMed: 15866891]
10. Liou J, Kim ML, Heo WD, Jones JT, Myers JW, Ferrell JEJ, Meyer T. STIM is a Ca^{2+} sensor essential for Ca^{2+}-store-depletion-triggered Ca^{2+} influx. Curr Biol. 2005; 15:1235–1241. [PubMed: 16005298]
11. Cheng KT, Ong HL, Liu X, Ambudkar IS. Contribution of TRPC1 and Orai1 to Ca^{2+} entry activated by store depletion. Adv Exp Med Biol. 2011; 704:435–449. [PubMed: 21290310]
12. Peng JB, Chen XZ, Berger UV, Vassilev PM, Tsukaguchi H, Brown EM, Hediger MA. Molecular cloning and characterization of a channel-like transporter mediating intestinal calcium absorption. J Biol Chem. 1999; 274:22739–22746. [PubMed: 10428857]
13. Hoenderop JG, van der Kemp AW, Hartog A, van de Graaf SF, van Os CH, Willems PH, Bindels RJ. Molecular identification of the apical Ca^{2+} channel in 1, 25-dihydroxyvitamin D3-responsive epithelia. J Biol Chem. 1999; 274:8375–8378. [PubMed: 10085067]
14. Cui J, Bian JS, Kagan A, McDonald TV. CaT1 contributes to the stores-operated calcium current in Jurkat T-lymphocytes. J Biol Chem. 2002; 277:47175–47183. [PubMed: 12361955]
15. Vanden Abeele F, Shuba Y, Roudbaraki M, Lemonnier L, Vanoverberghe K, Mariot P, Skryma R, Prevarskaya N. Store-operated Ca^{2+} channels in prostate cancer epithelial cells: function, regulation, and role in carcinogenesis. Cell Calcium. 2003; 33:357–373. [PubMed: 12765682]
16. Nguyen TD, Moody MW, Steinhoff M, Okolo C, Koh DS, Bunnett NW. Trypsin activates pancreatic duct epithelial cell ion channels through proteinase-activated receptor-2. J Clin Invest. 1999; 103:261–269. [PubMed: 9916138]
17. Jung SR, Kim MH, Hille B, Nguyen TD, Koh DS. Regulation of exocytosis by purinergic receptors in pancreatic duct epithelial cells. Am J Physiol, Cell Physiol. 2004; 286:C573–579. [PubMed: 14602582]
18. Kim MH, Choi BH, Jung SR, Sernka TJ, Kim S, Kim KT, Hille B, Nguyen TD, Koh DS. Protease-activated receptor-2 increases exocytosis via multiple signal transduction pathways in pancreatic duct epithelial cells. J Biol Chem. 2008; 283:18711–18720. [PubMed: 18448425]
19. Jung SR, Kim MH, Hille B, Koh DS. Control of granule mobility and exocytosis by Ca^{2+}-dependent formation of F-actin in pancreatic duct epithelial cells. Traffic. 2009; 10:392–410. [PubMed: 19192247]

20. Jung SR, Seo JB, Shim D, Hille B, Koh DS. Actin cytoskeleton controls movement of intracellular organelles in pancreatic duct epithelial cells. Cell Calcium. 2012; 51:459–469. [PubMed: 22579052]
21. Oda D, Savard CE, Nguyen TD, Eng L, Swenson ER, Lee SP. Dog pancreatic duct epithelial cells: long-term culture and characterization. Am J Pathol. 1996; 148:977–985. [PubMed: 8774152]
22. Nguyen TD, Koh DS, Moody MW, Fox NR, Savard CE, Kuver R, Hille B, Lee SP. Characterization of two distinct chloride channels in cultured dog pancreatic duct epithelial cells. Am J Physiol. 1997; 272:G172–180. [PubMed: 9038891]
23. Nguyen TD, Okolo CN, Moody MW. Histamine stimulates ion transport by dog pancreatic duct epithelial cells through H1 receptors. 1998; 275:G76–84.
24. Palmer AE, Jin C, Reed JC, Tsien RY. Bcl-2mediated alterations in endoplasmic reticulum Ca^{2+} analyzed with an improved genetically encoded fluorescent sensor. Proc Natl Acad Sci USA. 2004; 101:17404–17409. [PubMed: 15585581]
25. Lewis RS, Ross PE, Cahalan MD. Chloride channels activated by osmotic stress in T lymphocytes. J Gen Physiol. 1993; 101:801–826. [PubMed: 7687269]
26. Novak I. Purinergic receptors in the endocrine and exocrine pancreas. Purinergic Signal. 2008; 4:237–253. [PubMed: 18368520]
27. Steward MC, Ishiguro H. Molecular and cellular regulation of pancreatic duct cell function. Curr Opin Gastroenterol. 2009; 25:447–453. [PubMed: 19571747]
28. Sorensen CE, Novak I. Visualization of ATP release in pancreatic acini in response to cholinergic stimulus. Use of fluorescent probes and confocal microscopy. J Biol Chem. 2001; 276:32925–32932. [PubMed: 11387334]
29. Zweifach A, Lewis RS. Slow calcium-dependent inactivation of depletion-activated calcium current. Store-dependent and -independent mechanisms. J Biol Chem. 1995; 270:14445–14451. [PubMed: 7540169]
30. Kerschbaum HH, Cahalan MD. Monovalent permeability, rectification, and ionic block of store-operated calcium channels in Jurkat T lymphocytes. J Gen Physiol. 1998; 111:521–537. [PubMed: 9524136]
31. Lewis RS, Cahalan MD. Mitogen-induced oscillations of cytosolic Ca^{2+} and transmembrane Ca^{2+} current in human leukemic T cells. Cell Regul. 1989; 1:99–112. [PubMed: 2519622]
32. Steward MC, Ishiguro H, Case RM. Mechanisms of bicarbonate secretion in the pancreatic duct. Annu Rev Physiol. 2005; 67:377–409. [PubMed: 15709963]
33. Putney JWJ. A model for receptor-regulated calcium entry. Cell Calcium. 1986; 7:1–12. [PubMed: 2420465]
34. Cahalan MD, Zhang SL, Yeromin AV, Ohlsen K, Roos J, Stauderman KA. Molecular basis of the CRAC channel. Cell Calcium. 2007; 42:133–144. [PubMed: 17482674]
35. Feske S, Gwack Y, Prakriya M, Srikanth S, Puppel SH, Tanasa B, Hogan PG, Lewis RS, Daly M, Rao A. A mutation in Orai1 causes immune deficiency by abrogating CRAC channel function. Nature. 2006; 441:179–185. [PubMed: 16582901]
36. Cahalan MD. STIMulating store-operated Ca^{2+} entry. Nat Cell Biol. 2009; 11:669–677. [PubMed: 19488056]
37. Huang GN, Zeng W, Kim JY, Yuan JP, Han L, Muallem S, Worley PF. STIM1 carboxyl-terminus activates native SOC, I_{crac} and TRPC1 channels. Nat Cell Biol. 2006; 8:1003–1010. [PubMed: 16906149]
38. Cahalan MD, Chandy KG. The functional network of ion channels in T lymphocytes. Immunol Rev. 2009; 231:59–87. [PubMed: 19754890]
39. Feske S. Calcium signalling in lymphocyte activation and disease. Nat Rev Immunol. 2007; 7:690–702. [PubMed: 17703229]
40. Liu YJ, Gylfe E. Store-operated Ca^{2+} entry in insulin-releasing pancreatic beta-cells. Cell Calcium. 1997; 22:277–286. [PubMed: 9481478]
41. Mogami H, Nakano K, Tepikin AV, Petersen OH. Ca^{2+} flow via tunnels in polarized cells: recharging of apical Ca^{2+} stores by focal Ca^{2+} entry through basal membrane patch. Cell. 1997; 88:49–55. [PubMed: 9019404]

42. Baba A, Yasui T, Fujisawa S, Yamada RX, Yamada MK, Nishiyama N, Matsuki N, Ikegaya Y. Activity-evoked capacitative Ca^{2+} entry: implications in synaptic plasticity. J Neurosci. 2003; 23:7737–7741. [PubMed: 12944501]
43. Emptage NJ, Reid CA, Fine A. Calcium stores in hippocampal synaptic boutons mediate short-term plasticity, store-operated Ca^{2+} entry, and spontaneous transmitter release. Neuron. 2001; 29:197–208. [PubMed: 11182091]
44. Prakriya M, Lewis RS. Potentiation and inhibition of Ca^{2+} release-activated Ca^{2+} channels by 2-aminoethyldiphenyl borate (2-APB) occurs independently of IP_3 receptors. J Physiol (Lond). 2001; 536:3–19. [PubMed: 11579153]
45. Lis A, Peinelt C, Beck A, Parvez S, Monteilh-Zoller M, Fleig A, Penner R. CRACM1, CRACM2, and CRACM3 are store-operated Ca^{2+} channels with distinct functional properties. Curr Biol. 2007; 17:794–800. [PubMed: 17442569]
46. Parvez S, Beck A, Peinelt C, Soboloff J, Lis A, Monteilh-Zoller M, Gill DL, Fleig A, Penner R. STIM2 protein mediates distinct store-dependent and store-independent modes of CRAC channel activation. FASEB J. 2008; 22:752–761. [PubMed: 17905723]
47. DeHaven WI, Smyth JT, Boyles RR, Bird GS, Putnery JWJ. Complex actions of 2-aminoethyldiphenyl borate on store-operated calcium entry. J Biol Chem. 2008; 283:19265–19273. [PubMed: 18487204]
48. DeHaven WI, Smyth JT, Boyles RR, Putney JWJ. Calcium inhibition and calcium potentiation of Orai1, Orai2, and Orai3 calcium release-activated calcium channels. J Biol Chem. 2007; 282:17548–17556. [PubMed: 17452328]
49. Gruszczynska-Biegala J, Pomorski P, Wisniewska MB, Kuznicki J. Differential roles for STIM1 and STIM2 in store-operated calcium entry in rat neurons. PLoS ONE. 2011; 6:e19285. [PubMed: 21541286]
50. Feske S, Prakriya M, Rao A, Lewis RS. A severe defect in CRAC Ca^{2+} channel activation and altered K^+ channel gating in T cells from immunodeficient patients. J Exp Med. 2005; 202:651–662. [PubMed: 16147976]
51. Shuttleworth TJ. Orai3- the 'exceptional' Orai? J Physiol (Lond). 2012; 590:241–257. [PubMed: 22041188]
52. Kerstan D, Thomas J, Nitschke R, Leipziger J. Basolateral store-operated Ca^{2+}-entry in polarized human bronchial and colonic epithelial cells. Cell Calcium. 1999; 26:253–260. [PubMed: 10668563]
53. Hong JH, Li Q, Kim MS, Shin DM, Feske S, Birnbaumer L, Cheng KT, Ambudkar IS, Muallem S. Polarized but differential localization and recruitment of STIM1, Orai1 and TRPC channels in secretory cells. Traffic. 2011; 12:232–45. [PubMed: 21054717]
54. Sutton R, Petersen OH, Pandol SJ. Pancreatitis and calcium signalling: report of an international workshop. Pancreas. 2008; 36:e1–14. [PubMed: 18437073]

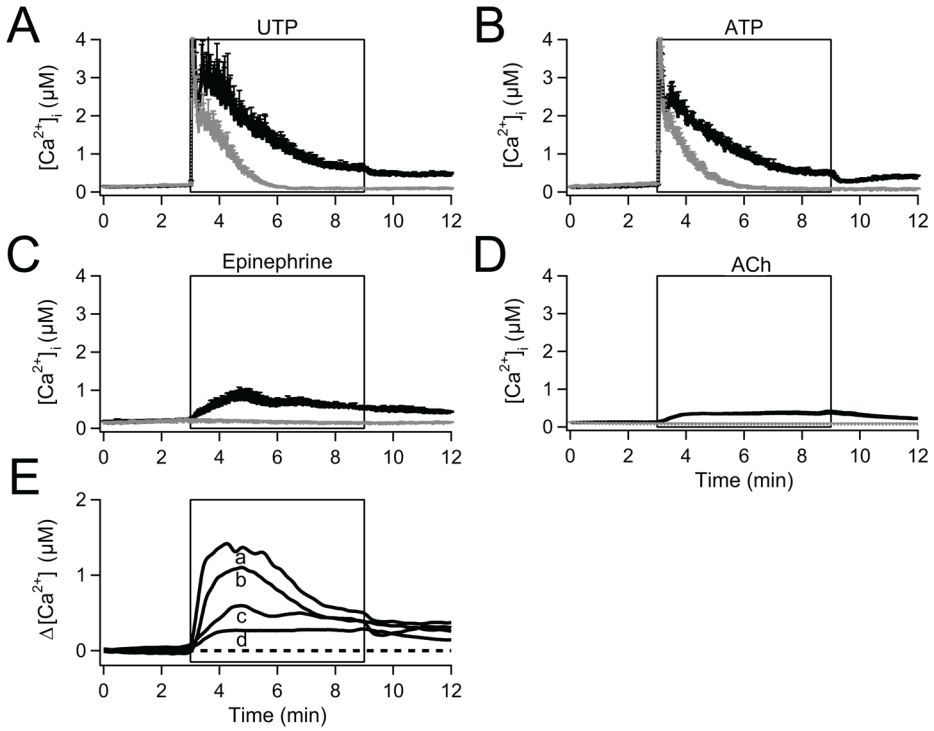

Fig. 1.

Activation of SOC by physiological agonists applied to isolated PDEC. Traces are time courses of $[Ca^{2+}]_i$ measured ratiometrically using Fura-2. (A) Averaged $[Ca^{2+}]_i$ increase evoked by 100 μM UTP with (black line, $n = 10$) and without Ca^{2+} in the bathing medium (gray line, $n = 10$). (B) Similar experiments with 100 μM ATP ($n = 8$, black line; $n = 8$, gray line). (C) 1 μM epinephrine ($n = 5$, black line; $n = 4$, gray line). (D) 100μM acetylcholine (ACh; $n = 20$, black line; $n = 16$, gray line). (E) Difference $[Ca^{2+}]_i$ traces (with-Ca^{2+} minus without-Ca^{2+}) reflecting the relative contribution of Ca^{2+} influx calculated for UTP (a), ATP (b), epinephrine (c), and acetylcholine (d). The broken line indicates the base level.

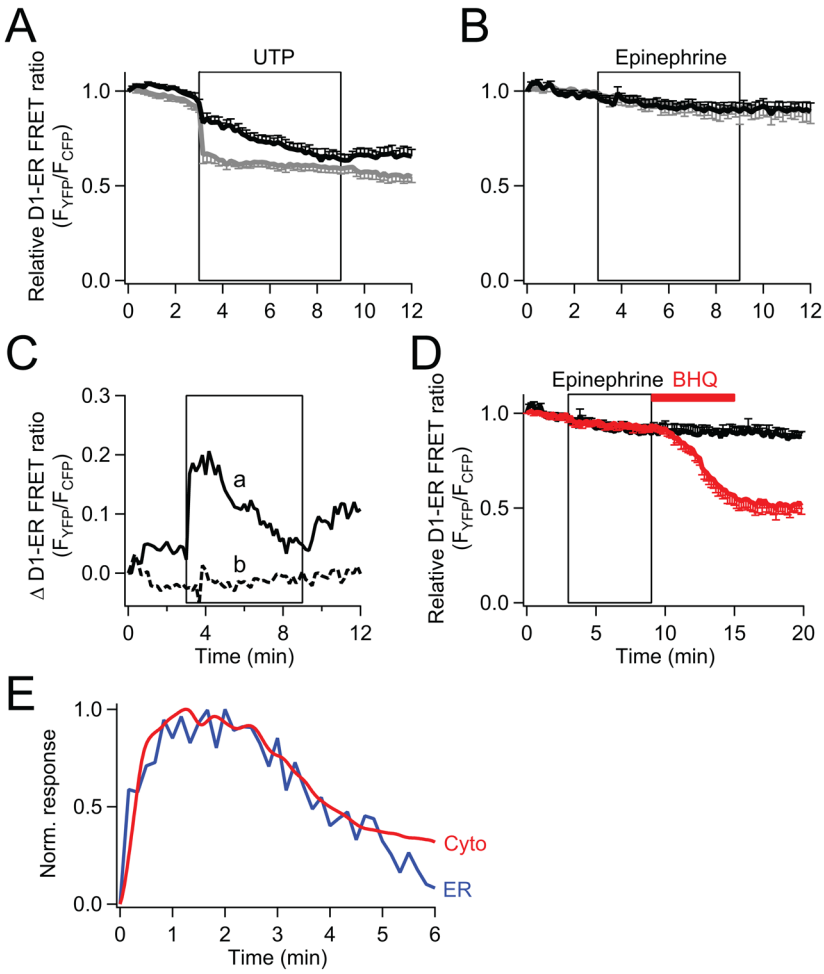

Fig. 2.

Comparison of the activation of store depletion by UTP and epinephrine. $[Ca^{2+}]_{ER}$ in single PDEC, measured by FRET with D1-ER cameleon as the $[Ca^{2+}]_{ER}$ sensor. (A) Time course of relative (normalized) $[Ca^{2+}]_{ER}$ during addition of 100 μM UTP in either normal Ringer's ($n = 7$, black line) or Ca^{2+}-free Ringer's ($n = 8$, gray line). (B) Activation of SOC triggered by 1 μM epinephrine treatment (same experimental protocol as in (A)) with normal external Ringer's ($n = 7$, black line) and Ca^{2+}-free Ringer's ($n = 5$, gray line). (C) Comparison of the SOC contribution to $[Ca^{2+}]_{ER}$ during 100 μM UTP (a, solid line) and 1 μM epinephrine (b, dotted line) treatment. The values are calculated as the difference between the $[Ca^{2+}]_{ER}$ traces in external Ringer's solution with and without Ca^{2+} shown in (A) and (B). (D) Black trace, 1 μM epinephrine is followed by Ringer's wash (same data as in (B)). Red trace, 50 μM BHQ was applied after the epinephrine treatment (9–15 min time period) in normal external Ringer's solution ($n = 10$). (E) Activation kinetics of the SOC contribution to cytoplasmic Ca^{2+} rises ("Cyto", red line, from Fig. 1E trace a), and ER Ca^{2+} rises ("ER", blue line, from Fig. 2C trace a). The responses are normalized to their peak values.

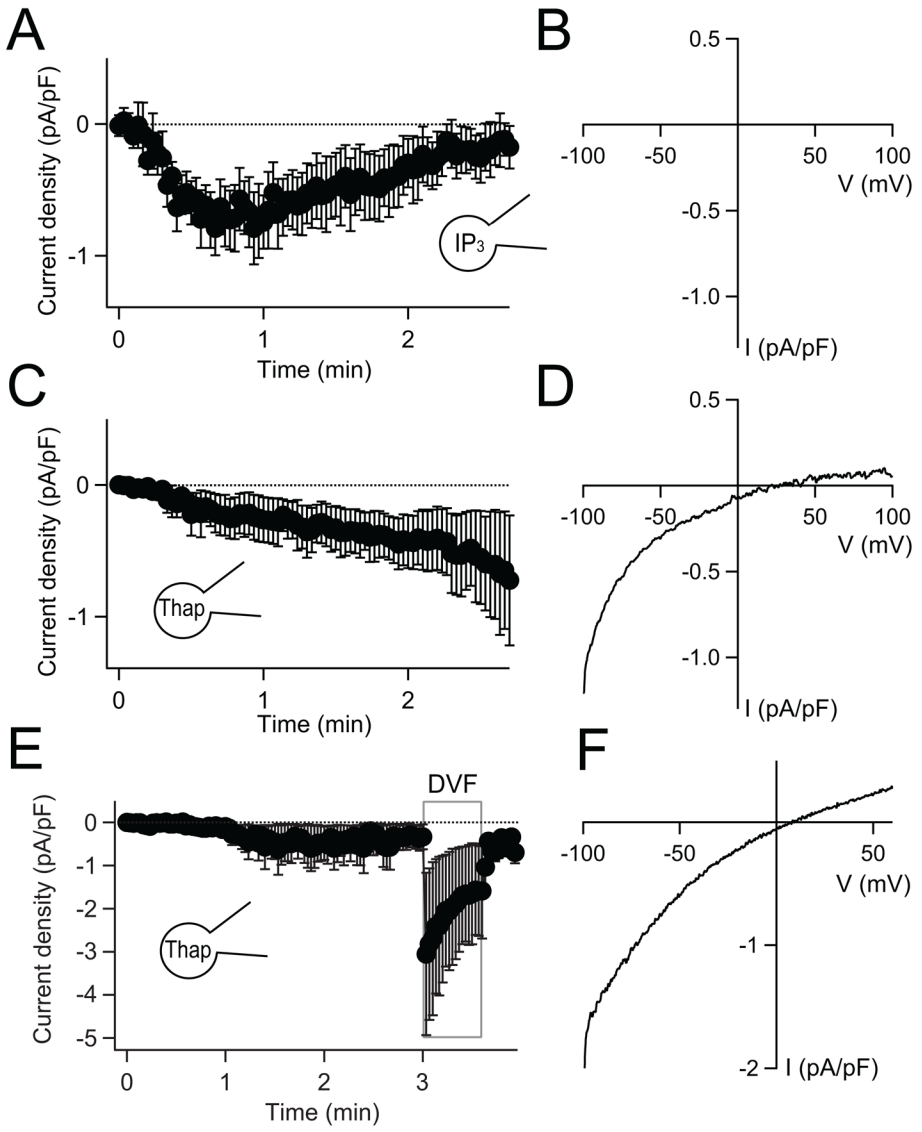

Fig. 3.

Activation of SOC current by depletion of Ca^{2+} stores. (A) Average time course of whole-cell current density at −100 mV with 100 μM IP_3 and 10 mM EGTA in the pipette solution ($n = 5$). External solution contained 20 mM Ca^{2+}. Current density is current (pA) divided by cell area (as cell capacity, pF). (B) A representative current-voltage relation of the whole-cell currents derived from a ramp protocol recorded after reaching maximal current activation. (C) and (D) The same protocol as in (A) and (B) but 100 μM IP_3 was substituted for 5 μM thapsigargin in the pipette solution ($n = 5$). (E) SOC currents at −100 mV in normal Ringer's solution with 2 mM Ca^{2+} and in external divalent-free Ringer's solution (DVF) ($n = 3$). The patch-pipette solution contains 5 μM thapsigargin. (F) Representative current-voltage relation for maximal SOC current in DVF. The initial current densities recorded at −100 mV immediately after establishment of whole-cell configuration were subtracted in the traces shown in (A), (C), and (E).

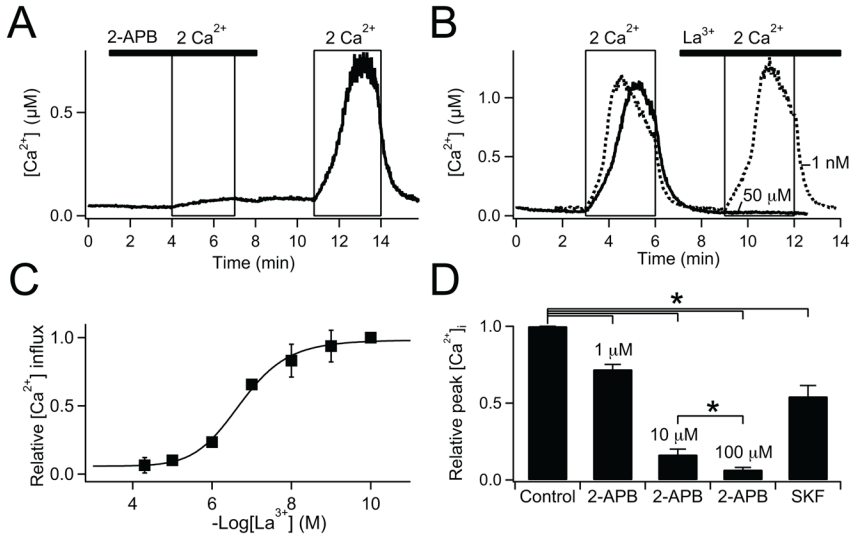

Fig. 4.

Pharmacological block of SOC in PDEC. Single-cell Ca^{2+}-photometry shown in (A) and (B), and summarized data shown in (C) and (D). (A) Cells were pretreated with 5 μM thapsigargin for 5 min to deplete the Ca^{2+} stores in Ca^{2+}-free Ringer's. Ca^{2+} influx through SOC, upon the switch to 2 mM external Ca^{2+}, was blocked by 100 μM 2-APB (bar) ($n = 6$, (A)) and 50 μM La^{3+} (bar) ($n = 3$, solid line in (B)), but not, 1 nM La^{3+} ($n = 3$, dotted line in (B)). (C) Dose response curve for La^{3+}-mediated block of Ca^{2+} influx (IC_{50} = 199 nM, n = 3–7 for each concentration). (D) Block of Ca^{2+} influx by SOC blockers, 1, 10, 100 μM 2-APB (n = 11, 8, 6), and 50 μM SKF-96365 ($n = 3$). Peak $[Ca^{2+}]_i$ values achieved by 2 mM external Ca^{2+} in the presence of blockers compared to control. The same experimental protocol was used as for (A). $P^* < 0.05$.

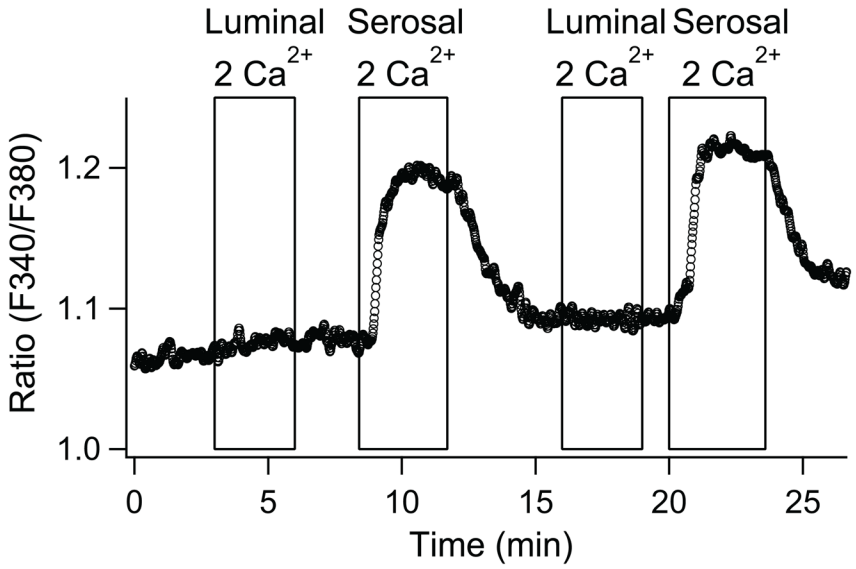

Fig. 5.

Localization of SOCs to the basolateral side of polarized PDEC. Representative of 4 experiments. A differentiated PDEC monolayer were pretreated with 5 μM thapsigargin for 5 min in Ca^{2+}-free Ringer's. External 2 mM Ca^{2+}-containing solution was applied to either luminal/apical or serosal/basolateral sides of PDEC. $[Ca^{2+}]_i$ is expressed as the fluorescence ratio at 340 and 380 nm.

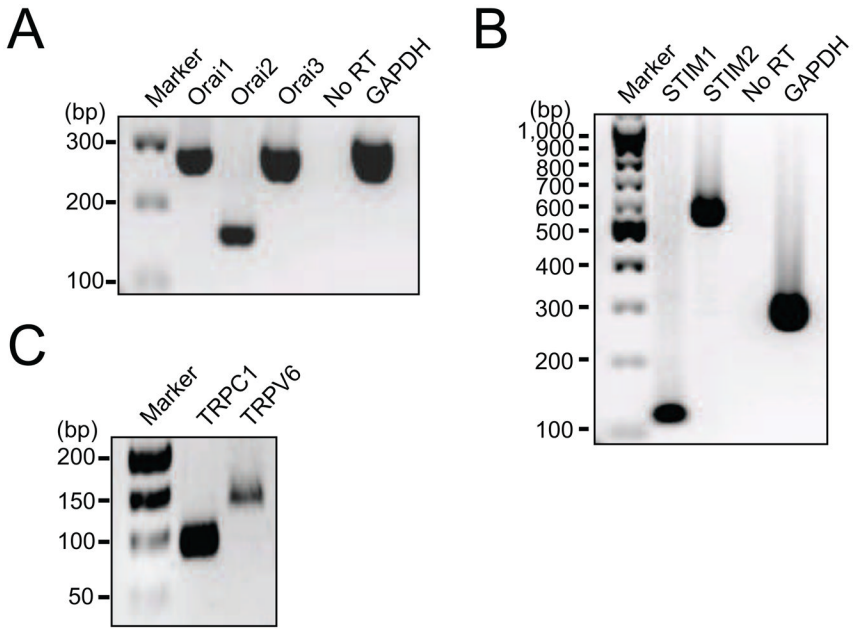

Fig. 6.

Expression of Orai, STIM, and TRP in dog PDEC. Reverse transcription-PCR screening for Orai1, Orai2, and Orai3 (A), STIM1 and STIM2 (B), and TRPC1 and TRPV6 (C). PCR products were electrophoresed in 2% agarose gels and detected as single bands at the expected molecular weights. Similar results were obtained in three independent experiments.

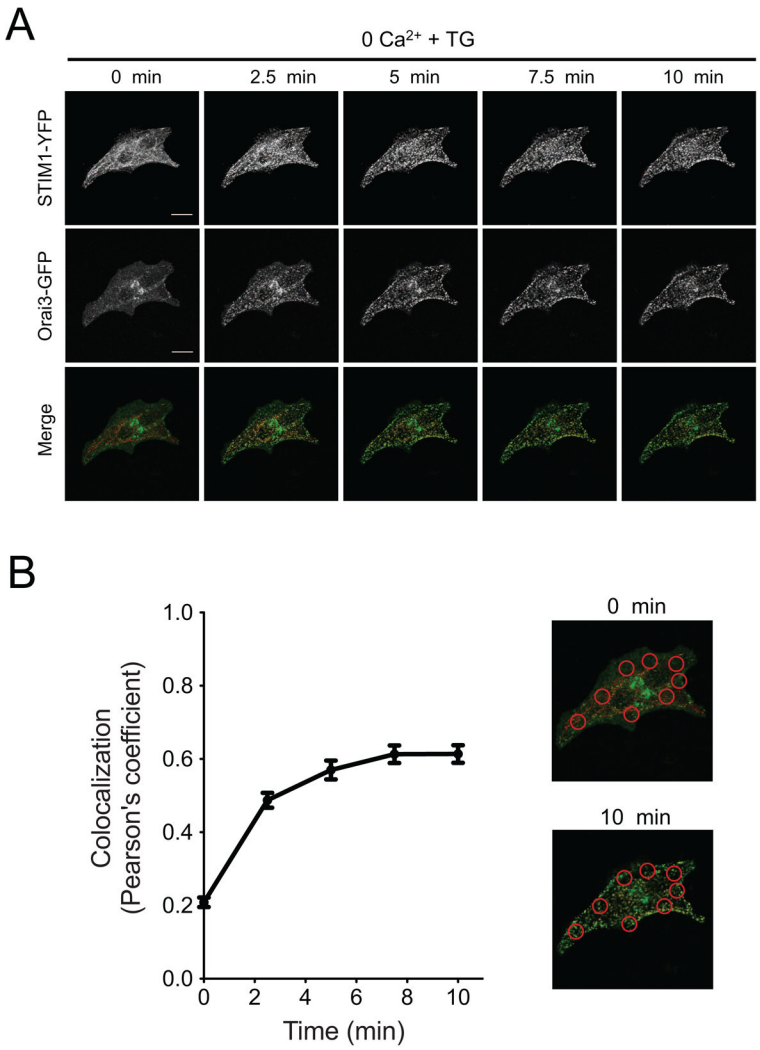

Fig. 7.

Puncta formation and their colocalization for STIM1 and Orai3 proteins in single dissociated PDEC assessed with confocal microscopy. (A) STIM1 and Orai3 form colocalized puncta after store depletion. Images in the first column (0 min) were obtained with normal Ringer's solution, and then cells were treated with 5 μM thapsigargin in Ca^{2+}-free external Ringer's solution for 10 min. In the merged images, STIM1-YFP is color coded as red and Orai3-GFP as green. White scale bar indicates 20 μm. (B) Colocalization between STIM1 and Orai3 channels was calculated before and after store depletion (n = 5, 8 regions of interest per cell). ROIs used for the colocalization analysis are indicated in the merged images.

Table 1

Primer sets used for RT-PCR analysis. Expected transcript sizes are indicated in the right column.

Gene	Forward primer	Reverse primer	GenBank Accession number	Exp. size (bp)
Orai1	CACTGTCATTGGCACACTCC	CCGTTTTATGGCTGACCAGT	XM_543386	272
Orai2	AGCGGTAGAAGTGGATGGTG	TGCTGGATCAAGTTCCTTCC	XM_845012	157
Orai3	GCTGGAGAGCAACCATGAAT	ACAAACTTGACCCAGCCAAC	XM_843928	276
STIM1	GGATGTGTGCGCCCGTGTTG	TCCTCAGAAGTAGCCCCTGAGCCA	XM_003433013	123
STIM2	CTGTTTCAGATCCCTGCCTGTCACT	ACGCAAACCAGCACCCTCCAAC	XM_536267	561
TRPC1	CGTGCGACAAGGGTGACTAT	CTCCCAAGCACATCTACGCA	XM_003639831	94
TRPC3	CACAGCAGTACGTGGACAGT	ATGCGATCCGAGAGAAGCTG	XM_540964	174
TRPC4	GGCGGGCTGCTGATAATTTG	GAGGCAATTGCTGCTGATCG	XM_543129	355
TRPV6	CTCAGAGCCGAGATGAGCAG	TCCTTTCTCGTGCACCTCAC	XM_539861	140
GAPDH	GGTGATGCTGGTGCTGAGTA	GTCTTCTGGGTGGCAGTGAT	AB038240	299